Momentum Entanglement for Atom Interferometry

F. Anders,[1,*] A. Idel,[1] P. Feldmann,[2] D. Bondarenko,[2] S. Loriani,[1] K. Lange,[1] J. Peise,[1] M. Gersemann,[1] B. Meyer-Hoppe,[1] S. Abend,[1] N. Gaaloul,[1] C. Schubert,[1,3] D. Schlippert,[1] L. Santos,[2] E. Rasel,[1] and C. Klempt[1,3]

[1]*Institut für Quantenoptik, Leibniz Universität Hannover, Welfengarten 1, D-30167 Hannover, Germany*

[2]*Institut für Theoretische Physik, Leibniz Universität Hannover, Appelstraße 2, D-30167 Hannover, Germany*

[3]*Deutsches Zentrum für Luft- und Raumfahrt e.V. (DLR), Institut für Satellitengeodäsie und Inertialsensorik, c/o Leibniz, Universität Hannover, DLR-SI, Callinstraße 36, 30167 Hannover, Germany*

(Received 30 November 2020; accepted 3 September 2021; published 29 September 2021)

Compared to light interferometers, the flux in cold-atom interferometers is low and the associated shot noise is large. Sensitivities beyond these limitations require the preparation of entangled atoms in different momentum modes. Here, we demonstrate a source of entangled atoms that is compatible with state-of-the-art interferometers. Entanglement is transferred from the spin degree of freedom of a Bose-Einstein condensate to well-separated momentum modes, witnessed by a squeezing parameter of $-3.1(8)$ dB. Entanglement-enhanced atom interferometers promise unprecedented sensitivities for quantum gradiometers or gravitational wave detectors.

DOI: 10.1103/PhysRevLett.127.140402

Atom-interferometric measurements are fundamentally restricted by the standard quantum limit (SQL), which can only be overcome by employing entangled atomic ensembles. Surpassing the SQL with measurements based on internal degrees of freedom has been demonstrated in many different systems [1] at room temperature [2], in ultracold ensembles [3–6], and in Bose-Einstein condensates (BECs) [7–14]. However, momentum-entangled sources as required for atom interferometers present a long-standing challenge.

Controlled atomic collisions were shown to enable the generation of entanglement between spatial modes [15–19], as well as correlated and entangled atomic pairs in momentum space [20–22]. However, the demonstrations involve specific momentum or spatial modes, which cannot be chosen freely. The efficient integration of these modes in state-of-the-art atom interferometers typically operating with Raman or Bragg transitions implies a considerable challenge. Alternative approaches working with well-suited momentum modes have so far only been proposed theoretically [23–28].

In this Letter, we report on a source for momentum-entangled atoms featuring the excellent mode quality of a Bose-Einstein condensate. We achieve this by the transfer of entangled twin-Fock states in the spin degree of freedom of a BEC to momentum space (Fig. 1). The twin-Fock states are created in a trap and released into free space, where one of the twin modes is coherently transferred to a well-separated momentum mode. Between the two momentum modes, we record number and phase fluctuations and obtain a spin squeezing parameter [29] of $-3.1(8)$ dB, which proves entanglement in momentum space. The demonstrated entanglement is directly

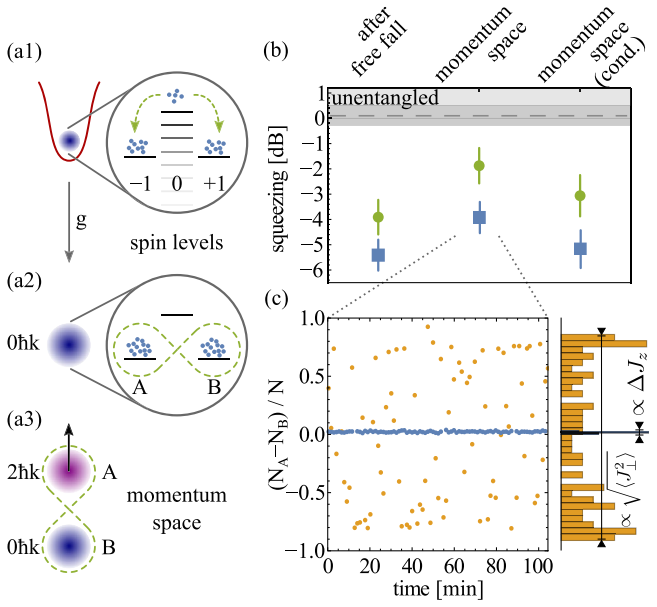

FIG. 1. Entanglement in momentum space. (a1) In a trap, spin-changing collisions create entangled atomic ensembles in two spin levels. (a2) The entanglement is maintained during free fall and (a3) transferred to two distinct momentum modes. (b) Measured number squeezing $4(\Delta J_z)^2/N$ (blue squares) and squeezing parameter [29] (green dots) after free fall, in momentum space, and conditionally (see text). Values are well below the classical limit of 0 dB, which is experimentally verified with a coherent spin state (gray dashed line, uncertainty as dark gray area). (c) Measured atom number differences before (blue) and after (orange) $\pi/2$ coupling. Before the coupling, the two modes A and B are equally populated and yield ultralow fluctuations in the number difference. After the coupling, the fluctuations are large, with a characteristic cumulation at extreme values. Each set of data points in (b) is derived from such data.

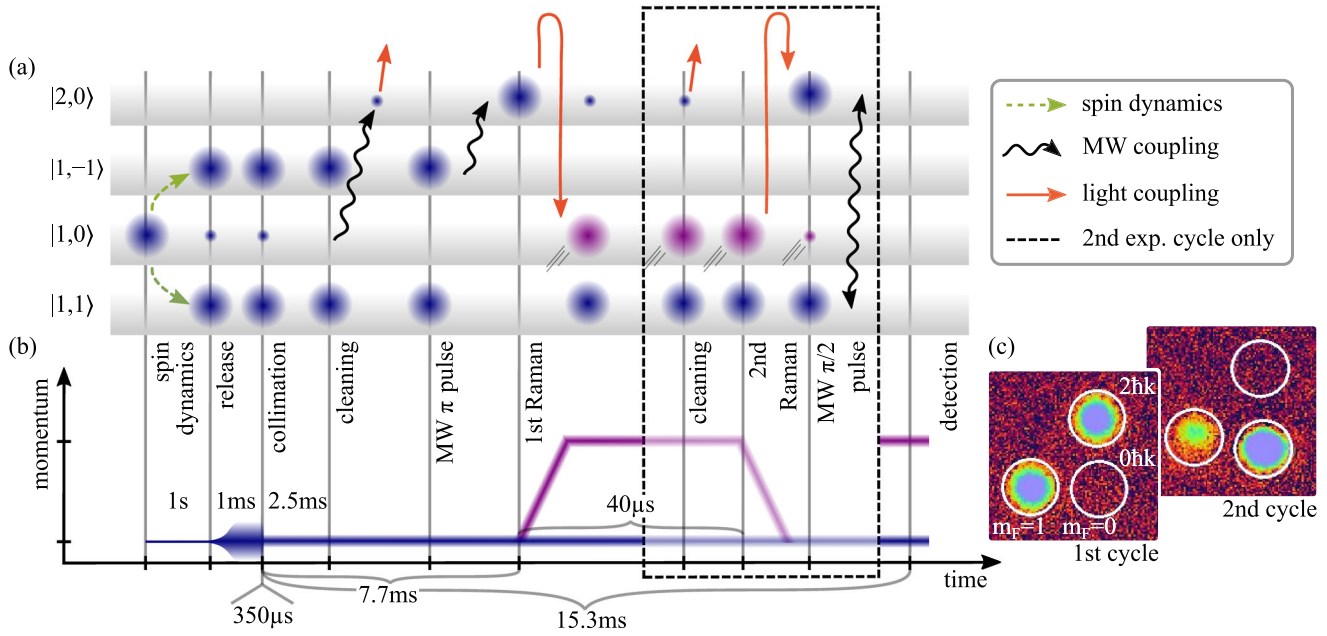

FIG. 2. Schematic overview of the experimental sequence. (a) The transfer of atoms between the various involved spin states. The type of coupling is indicated by different arrows (legend). We measure J_z and $J_\perp$ in two alternating measurement cycles. Operations enclosed by the dashed rectangle only take place in the second cycle to measure $J_\perp$. (b) The time-momentum diagram shows the effect on the momentum mode of the atomic cloud in the free-falling reference frame (axes not to scale). (c) Typical absorption images taken at the end of both cycles.

applicable in existing atom interferometers to enable sensitivities beyond the SQL [27,30]. Such a quantum-enhanced resolution is of vital interest for future large-scale atom interferometers that measure relative observables, for Earth observation gradiometry [31], for tests of the Einstein Equivalence Principle [32–35], and for the proposed terrestric [36–39] and space-borne [40–44] gravitational wave detectors. Momentum-entangled atoms further constitute a promising probe for tests of fundamental decoherence [45] and tests of Bell nonlocality with massive particles [46,47].

We initiate our experiments by the preparation of entangled states in spin space. A BEC of 10^4 ^{87}Rb atoms is produced in a crossed-beam optical dipole trap with trapping frequencies of $2\pi \times (150, 160, 220)$ Hz. The atoms are prepared in the hyperfine level $|F, m_F\rangle = |1, 0\rangle$ at an actively stabilized, homogeneous magnetic field of 0.73 G oriented parallel to the gravitational acceleration. We employ spin-changing collisions [30,48,49] to generate entangled twin-Fock states $|N_A = N/2\rangle \otimes |N_B = N/2\rangle$ in the two levels $m_F = \pm 1$. Following earlier work [50–52], we generate these states by a quasiadiabatic crossing of a quantum phase transition. In our realization, we apply an intensity-stabilized homogeneous microwave (MW) field, which is blue detuned by 400 kHz from the transition $|1, 0\rangle \leftrightarrow |2, 0\rangle$, and linearly ramp the field intensity. Without MW dressing, an atom pair in $|1, \pm 1\rangle$ has a relative energy of $q = h \times 38.5$ Hz/atom compared to a pair in $|1, 0\rangle$ due to the quadratic Zeeman shift. For the initial spin orientation, the BEC in $|1, 0\rangle$ is thus in the many-body ground state of the system. We then apply a 1020 ms linear intensity ramp to the dressing field, which lowers the energy of the $|1, \pm 1\rangle$ levels to $-h \times 5$ Hz each (see Supplemental Material [53]). The atoms follow the ground state of the system toward a twin-Fock state at the end of the ramp. Despite experimental noise and finite ramping speed, 93(5)% of the atoms are transferred to the levels $|1, \pm 1\rangle$. Slower ramps allow for even higher transfer efficiencies. However, the fraction of leftover atoms is sufficiently small to be removed without disturbing the ensemble. To reduce decoherence, we prefer moderate holding times to maximum transfer efficiency. The overall preparation yields a total of $\langle N \rangle = 9300$ atoms with only 10% relative fluctuations, which are prepared in an entangled twin-Fock state in the spin degree of freedom.

The transfer to momentum space requires a release to free space without destruction of the entanglement (the full sequence is displayed in Fig. 2). The trapping laser fields are switched off instantaneously to initiate a free expansion, which is dominated by mean-field interaction [58]. This accelerated expansion turns quickly into a ballistic expansion after the density has dropped. Because of the initial high density, necessary to generate entanglement via spin-changing collisions, the out-coupled cloud has a broad velocity distribution of 1.8 mms^{-1} (rate of change of the standard deviation of a Gaussian fit). However, a narrow velocity distribution is favorable for the acceleration by a stimulated Raman transition to avoid Doppler shifts (along

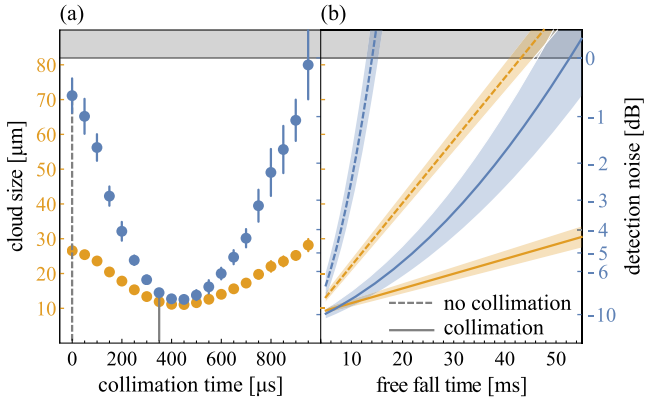

FIG. 3. Effect of the collimation on cloud size (orange, left scale) and detection noise (blue, right scale). (a) At a fixed free-fall time of 13 ms after the collimation, the size of the atomic cloud is measured as a function of the collimation pulse time. The cloud size determines the minimal number of relevant pixels on the CCD camera. This corresponds to a minimal detection noise, which we compare to shot noise (gray area). (b) Extrapolation to longer free-fall times based on expansion rates measured for the two settings marked by vertical lines in (a). Shaded areas represent the uncertainty of the extrapolation. The maximal free-fall time allowing for sub-shot-noise detection is increased by a factor of 3.7 to about 50 ms.

the Raman-beam direction) and the sensing of phase and intensity gradients (along transverse directions). Furthermore, a broad velocity distribution would be converted into an extended spatial distribution. We therefore apply a three-dimensional collimation pulse [59]. After 1 ms of free fall, we flash the dipole trapping field with its original strength for an adjustable duration. Figure 3 shows the effect of this collimation. For an increasing collimation pulse length, the detected cloud size is first reduced, reaches a minimum, and increases again. In our experiments, we choose a pulse length of 350 μs to obtain collimated clouds, as they are desirable for long interrogation times in the future. The reduction of the cloud size is also essential for its detection with sub-shot-noise sensitivity [60]. Extended clouds require more pixels on the final absorption images and thereby sample more noise. Without collimation, the detection noise would remain at suitably low values only for a few milliseconds of free-fall time. From Fig. 3(b), we extract that the collimation reduces the detection noise from 0.5 to −6.7 dB at our typical free-fall time of 15 ms, and it therefore actually enables a transfer of entanglement to momentum space and its subsequent detection [61].

After the collimation, the clouds slowly expand for another 2.5 ms to be sufficiently dilute to remove the remaining atoms from the level $|1,0\rangle$ by a MW transfer and a resonant light pulse. We detect no leftover atoms and, after another MW transfer (Fig. 2), a clean, free-falling twin-Fock state in the levels $|1,1\rangle$ and $|2,0\rangle$ remains.

We evaluate the quality of the twin-Fock state of spin levels after 15 ms free fall subsequent to the collimation. Analogous to prior work [9,60], we detect the number of atoms $N_{A/B}$ in the two modes $|0\hbar k;1,1\rangle$ and $|0\hbar k;2,0\rangle$ and observe strongly reduced fluctuations. Figure 1(b) shows the obtained number squeezing $4(\Delta J_z)^2/N$ of 5.4(6) dB below shot noise (limited by detection noise). A detection of entanglement requires the measurement of a conjugate observable such as the relative phase. Here, the phase can be observed after performing a symmetric $\pi/2$ MW coupling pulse between the two modes. The two measurements are combined in a squeezing parameter [29] $\xi^2 = (\Delta J_z)^2/[2\langle J_\perp^2/(\hat{N}-1)\rangle - \langle(\hat{N}/2)/(\hat{N}-1)\rangle]$, where $(\Delta J_z)^2$ represents the variance of the number difference $J_z = \frac{1}{2}(\hat{N}_A - \hat{N}_B)$ and $\langle J_\perp^2\rangle$ is the second moment of the same number difference after the $\pi/2$ rotation [Fig. 1(c)]. The squeezing parameter proves entanglement if $\xi^2 < 1$. From our measurements in free fall, we obtain a squeezing parameter of −3.9(7) dB with respect to the classical bound $\xi^2 = 1$. The number squeezing after free fall deteriorates only by 0.6 dB compared to quasiadiabatically produced twin-Fock states measured directly after release from the trap. The reduced fluctuations after rotation [69% of the ideal twin-Fock value of $\langle J_\perp^2\rangle = N/2(N/2+1)$] can be explained by decoherence due to longer holding times in the trap and asymmetries of the collimation procedure, which may lead to nonidentical spatial phase patterns for the two modes. We obtain a clear signal of entanglement in free-falling BECs, which presents a central result of this publication. In a complementary Letter, squeezed samples of thermal atoms were successfully released to a free fall of 8 ms [62].

The central development for achieving momentum entanglement is a high-efficiency momentum transfer. This is achieved with resonant Raman laser pulses that couple the levels $|2,0\rangle$ and $|1,0\rangle$ by a two-photon transition with 1.1 GHz red detuning from the $5P_{3/2}$ manifold. The pulses are temporally shaped with $\sin^2$ edges to reduce the frequency selectivity in Fourier space. Two separate diode lasers are used where the phase of the laser that couples to $|1,0\rangle$ (laser 1) is stabilized to the $|2,0\rangle$ laser (laser 2) [63]. The phase-stabilized beams are superposed with crossed linear polarizations and mode cleaned by an optical fiber. After the first fiber, the beam is switched by a single acousto-optical modulator and delivered to the experimental chamber via a second optical fiber. The intensity ratio is adjusted to a value of $I_2/I_1 = 0.93$ (in front of the atoms), where the AC stark shift (Autler-Townes effect) induced by both frequencies compensate, such that the Raman coupling is insensitive to fluctuations of the total power (< 1 mW per beam and a $1/e^2$ width of 1.5 mm). After out-coupling along the vertical direction, the Raman beams are given opposite circular polarizations and pass the falling cloud [Fig. 4(a)]. Below the cloud, laser beam 1 is removed,

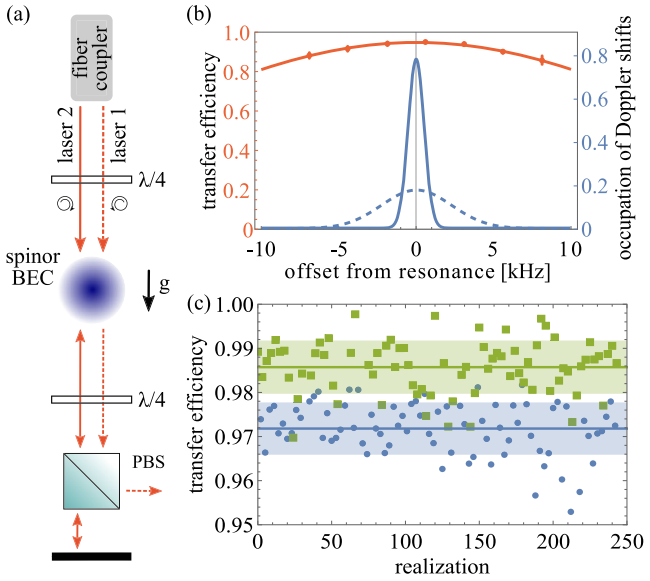

FIG. 4. Design and characterization of the Raman coupling scheme. (a) Schematic of the optical setup for realizing Raman transitions. Two oppositely circular-polarized phase-locked Raman beams (lasers 1 and 2) pass the atomic cloud from above. Because of selection by a polarizing beam splitter (PBS), only laser 2 is retroreflected. Thereby, only one pair of beams enables a momentum transfer of $2\hbar k$ and unwanted transfers are suppressed. The setup is chosen to ensure high relative phase stability of both laser beams and to allow for future measurements of gravity by alignment with the gravitational acceleration g. (b) Raman spectroscopy of the clock transition. The experimental data of the spectroscopy (orange data points and fit) are compared to the distributions of Doppler shifts due to the velocity spread before and after collimation (blue dashed and solid line). (c) Transfer efficiencies for two consecutive Raman pulses from $|2,0\rangle$ to $|1,0\rangle$ (blue circles) and back (green dots).

and laser beam 2 is reflected back to the atoms. The combination of laser 1 from above and laser 2 from below enables an upward acceleration by two-photon recoil quanta (11.8 mms^{-1}) that is associated with a spin transfer from $|1,0\rangle$ to $|2,0\rangle$. The obtained change of velocity is a factor of 29(3) larger than the velocity distribution of the cloud with a rms width of 0.41(4) mms^{-1}, enabling a clean preparation of distinct momentum modes. The Raman pulses are applied after 7.7 ms free fall of the collimated ensembles, because the gravitational acceleration to 76 mms^{-1} provides a sufficient Doppler shift to suppress unwanted transitions due to imperfect polarization and reflection.

We validate the efficiency of the Raman coupling by applying it to a free-falling BEC in the level $|2,0\rangle$. Figure 4(b) shows a spectroscopy of the Raman transition (orange) and compares it to the Doppler shifts due to the residual velocity spread (blue). The collimation reduces the ballistic expansion by 77% corresponding to a Doppler spread of 0.52(5) kHz (less than 1% of the Fourier width of the Raman pulse), equivalent to an effective temperature of 1.7(3) nK. The residual expansion rate is sufficiently small enough not to reduce the efficiency of the Raman coupling. Figure 4(c) shows the transfer efficiency for a transition from $|0\hbar k;2,0\rangle$ to $|2\hbar k;1,0\rangle$ (upward acceleration, blue) and a subsequent transition back to $|0\hbar k;2,0\rangle$ (downward acceleration, green). The transfer pulses yield an efficiency of 97.2(6)% and 98.5(6)%, respectively. We attribute the efficiency limitation to two main effects: (i) Because of finite temperature, there will be a small fraction of atoms with larger velocities that are not transferred due to the Doppler shift. Characteristically, this effect is strongly reduced for the second pulse, where the fast atoms have already been removed. (ii) Relative drifts of the Raman-beam intensities, as observed in our experiment, drive the system away from the ideal AC-Stark suppression. Therefore, depending on the elapsed time since the last calibration, the intensity fluctuations start to couple more to the resonance frequency, eventually reducing the efficiency. This effect is relevant for many hours of measurements and could be circumvented by an improved intensity stabilization in the future. However, the recorded efficiencies belong to the best reported Raman transfers [64–66] and constitute the main technical achievement to successfully transfer entangled states to different momentum modes [67]. Note that we take all atoms of the prepared state into account, without any velocity selection before the momentum transfer.

The described concepts can now be combined to prove entanglement in momentum space. We apply the Raman transfer to our twin-Fock state by coupling atoms in $|0\hbar k;2,0\rangle$ to a finite momentum state $|2\hbar k;1,0\rangle$. After an additional free-fall time of 7.6 ms, we detect two clouds clearly separated by 80(1) μm (center of mass). A strong magnetic field gradient in horizontal direction enables an independent detection of the unaffected atoms in $|0\hbar k;1,1\rangle$ and the small amount of leftover atoms in $|0\hbar k;2,0\rangle$ that stems from the imperfect Raman transfer. For the two macroscopically occupied clouds that drift apart, we record $-3.9(6)$ dB number squeezing (limited by fluctuations of the Raman transfer). If the measurement of the leftover atoms is exploited to predict the measurement outcome, thereby creating a conditional Dicke state, we obtain a number squeezing of $-5.2(7)$ dB [70]. In order to record the phase difference as a conjugate observable, we reverse the momentum transfer before the clouds separate substantially. Within 40 μs after the first Raman transfer, another cleaning procedure removes the leftover atoms in $|0\hbar k;2,0\rangle$ and a second Raman coupling decelerates the atoms back to $|0\hbar k;2,0\rangle$. Now, it is possible to couple the two twin-Fock modes by a MW $\pi/2$ pulse. Again, after a total free fall of 15 ms subsequent to the collimation, we obtain large fluctuations in the number difference, with a corresponding second moment of $\langle J_\perp^2\rangle = 0.63(5) \times N/2(N/2-1)$ and calculate a squeezing parameter of $-1.9(7)$ dB. For the conditional case, we obtain a

squeezing parameter of $-3.1(8)$ dB [Fig. 1(b) middle and right set of data points]. This proof of entanglement between two atomic modes, well separated in momentum space, presents our main result.

The observed entangled states are fully applicable for inertially sensitive atom interferometry beyond the SQL. For the desired quantum-enhanced phase sensitivity, the twin-Fock state must be rotated into the maximally phase-sensitive direction by an initial $\pi/2$ pulse. It is a characteristic advantage of the presented approach that these coupling pulses can be performed in the well-controlled spin space. Magnetic field insensitivity can be obtained by utilizing specific MW pulses to transfer both twin-Fock modes into the insensitive $m_F = 0$ states. In this case, a short Raman pulse can accelerate the modes in opposite directions with $4\hbar k$ momentum separation [66]. Alternatively, a long, velocity-selective Raman pulse could drive only one transition [63]. The presented scheme is not limited to twin-Fock states, but also applies to other entangled states in spin space, for example, spin-squeezed states [13,49]. The demonstrated source of entangled, Bose-condensed atoms in momentum space opens the path to operate future atom interferometers with quantum-enhanced sensitivities. This is specifically desirable for relative measurements with multiple atom interferometers, where some dominant technical noise sources like vibrational noise are suppressed by common-noise rejection.

We thank A. Smerzi and G. Tóth for valuable discussions and J. Arlt for a critical review of the Letter. We acknowledge support from the European Union through the QuantERA Grant No. 18-QUAN-0012-01 (CEBBEC). The work is funded by the Deutsche Forschungsgemeinschaft (DFG, German Research Foundation) under Germany's Excellence Strategy—EXC-2123 QuantumFrontiers—390837967, and through CRC 1227 (DQ-mat), projects A02 and B07. F. A. acknowledges support from the Hannover School for Nanotechnology (HSN). D. S. acknowledges support by the Federal Ministry of Education and Research (BMBF) through the funding program Photonics Research Germany under Contract No. 13N14875.

*Corresponding author.
anders@iqo.uni-hannover.de

[1] L. Pezzè, A. Smerzi, M. K. Oberthaler, R. Schmied, and P. Treutlein, Quantum metrology with nonclassical states of atomic ensembles, Rev. Mod. Phys. **90**, 035005 (2018).
[2] W. Wasilewski, K. Jensen, H. Krauter, J. J. Renema, M. V. Balabas, and E. S. Polzik, Quantum Noise Limited and Entanglement-Assisted Magnetometry, Phys. Rev. Lett. **104**, 133601 (2010).
[3] I. D. Leroux, M. H. Schleier-Smith, and V. Vuletic, Implementation of Cavity Squeezing of a Collective Atomic Spin, Phys. Rev. Lett. **104**, 073602 (2010).
[4] A. Louchet-Chauvet, J. Appel, J. J. Renema, D. Oblak, N. Kjaergaard, and E. S. Polzik, Entanglement-assisted atomic clock beyond the projection noise limit, New J. Phys. **12**, 065032 (2010).
[5] F. Haas, J. Volz, R. Gehr, J. Reichel, and J. Estève, Entangled states of more than 40 atoms in an optical fiber cavity, Science **344**, 180 (2014).
[6] O. Hosten, N. J. Engelsen, R. Krishnakumar, and M. A. Kasevich, Measurement noise 100 times lower than the quantum-projection limit using entangled atoms, Nature (London) **529**, 505 (2016).
[7] C. Gross, T. Zibold, E. Nicklas, J. Estève, and M. K. Oberthaler, Nonlinear atom interferometer surpasses classical precision limit, Nature (London) **464**, 1165 (2010).
[8] M. Riedel, P. Böhi, Y. Li, T. Hänsch, A. Sinatra, and P. Treutlein, Atom-chip-based generation of entanglement for quantum metrology, Nature (London) **464**, 1170 (2010).
[9] B. Lücke, M. Scherer, J. Kruse, L. Pezzé, F. Deuretzbacher, P. Hyllus, O. Topic, J. Peise, W. Ertmer, J. Arlt, L. Santos, A. Smerzi, and C. Klempt, Twin matter waves for interferometry beyond the classical limit, Science **334**, 773 (2011).
[10] C. F. Ockeloen, R. Schmied, M. F. Riedel, and P. Treutlein, Quantum Metrology with a Scanning Probe Atom Interferometer, Phys. Rev. Lett. **111**, 143001 (2013).
[11] H. Strobel, W. Muessel, D. Linnemann, T. Zibold, D. B. Hume, L. Pezzè, A. Smerzi, and M. K. Oberthaler, Fisher information and entanglement of non-Gaussian spin states, Science **345**, 424 (2014).
[12] W. Muessel, H. Strobel, D. Linnemann, D. B. Hume, and M. K. Oberthaler, Scalable Spin Squeezing for Quantum-Enhanced Magnetometry with Bose-Einstein Condensates, Phys. Rev. Lett. **113**, 103004 (2014).
[13] I. Kruse, K. Lange, J. Peise, B. Lücke, L. Pezzè, J. Arlt, W. Ertmer, C. Lisdat, L. Santos, A. Smerzi, and C. Klempt, Improvement of an Atomic Clock Using Squeezed Vacuum, Phys. Rev. Lett. **117**, 143004 (2016).
[14] Y.-Q. Zou, L.-N. Wu, Q. Liu, X.-Y. Luo, S.-F. Guo, J.-H. Cao, M. K. Tey, and L. You, Beating the classical precision limit with spin-1 Dicke states of more than 10,000 atoms, Proc. Natl. Acad. Sci. U.S.A. **115**, 6381 (2018).
[15] J. Estève, C. Gross, A. Weller, S. Giovanazzi, and M. K. Oberthaler, Squeezing and entanglement in a Bose-Einstein condensate, Nature (London) **455**, 1216 (2008).
[16] T. Berrada, S. van Frank, R. Bücker, T. Schumm, J.-F. Schaff, and J. Schmiedmayer, Integrated Mach-Zehnder interferometer for Bose-Einstein condensates, Nat. Commun. **4**, 2077 (2013).
[17] K. Lange, J. Peise, B. Lücke, I. Kruse, G. Vitagliano, I. Apellaniz, M. Kleinmann, G. Tóth, and C. Klempt, Entanglement between two spatially separated atomic modes, Science **360**, 416 (2018).
[18] M. Fadel, T. Zibold, B. Décamps, and P. Treutlein, Spatial entanglement patterns and Einstein-Podolsky-Rosen steering in Bose-Einstein condensates, Science **360**, 409 (2018).
[19] P. Kunkel, M. Prüfer, H. Strobel, D. Linnemann, A. Frölian, T. Gasenzer, M. Gärttner, and M. K. Oberthaler, Spatially distributed multipartite entanglement enables EPR steering of atomic clouds, Science **360**, 413 (2018).

[20] R. Bucker, J. Grond, S. Manz, T. Berrada, T. Betz, C. Koller, U. Hohenester, T. Schumm, A. Perrin, and J. Schmiedmayer, Twin-atom beams, Nat. Phys. **7**, 608 (2011).
[21] K. V. Kheruntsyan, J.-C. Jaskula, P. Deuar, M. Bonneau, G. B. Partridge, J. Ruaudel, R. Lopes, D. Boiron, and C. I. Westbrook, Violation of the Cauchy-Schwarz Inequality with Matter Waves, Phys. Rev. Lett. **108**, 260401 (2012).
[22] D. K. Shin, B. M. Henson, S. S. Hodgman, T. Wasak, J. Chwedeńczuk, and A. G. Truscott, Bell correlations between spatially separated pairs of atoms, Nat. Commun. **10**, 4447 (2019).
[23] L. Salvi, N. Poli, V. Vuletić, and G. M. Tino, Squeezing on Momentum States for Atom Interferometry, Phys. Rev. Lett. **120**, 033601 (2018).
[24] R. Geiger and M. Trupke, Proposal for a Quantum Test of the Weak Equivalence Principle with Entangled Atomic Species, Phys. Rev. Lett. **120**, 043602 (2018).
[25] A. Shankar, L. Salvi, M. L. Chiofalo, N. Poli, and M. J. Holland, Squeezed state metrology with Bragg interferometers operating in a cavity, Quantum Sci. Technol. **4**, 045010 (2019).
[26] S. S. Szigeti, S. P. Nolan, J. D. Close, and S. A. Haine, High-Precision Quantum-Enhanced Gravimetry with a Bose-Einstein Condensate, Phys. Rev. Lett. **125**, 100402 (2020).
[27] S. S. Szigeti, O. Hosten, and S. A. Haine, Improving cold-atom sensors with quantum entanglement: Prospects and challenges, Appl. Phys. Lett. **118**, 140501 (2021).
[28] R. Corgier, N. Gaaloul, A. Smerzi, and L. Pezzè, Delta-kick squeezing, arXiv:2103.10896.
[29] G. Vitagliano, I. Apellaniz, I. n. L. Egusquiza, and G. Tóth, Spin squeezing and entanglement for an arbitrary spin, Phys. Rev. A **89**, 032307 (2014).
[30] B. Lücke, M. Scherer, J. Kruse, L. Pezzé, F. Deuretzbacher, P. Hyllus, O. Topic, J. Peise, W. Ertmer, J. Arlt, L. Santos, A. Smerzi, and C. Klempt, Twin matter waves for interferometry beyond the classical limit, Science **334**, 773 (2011).
[31] M. J. Snadden, J. M. McGuirk, P. Bouyer, K. G. Haritos, and M. A. Kasevich, Measurement of the Earth's Gravity Gradient with an Atom Interferometer-Based Gravity Gradiometer, Phys. Rev. Lett. **81**, 971 (1998).
[32] D. N. Aguilera, H. Ahlers, B. Battelier, A. Bawamia, A. Bertoldi, R. Bondarescu, K. Bongs, P. Bouyer, C. Braxmaier, L Cacciapuoti, C. Chaloner, M. Chwalla, W. Ertmer, M. Franz, N. Gaaloul *et al.*, STE-QUEST—Test of the universality of free fall using cold atom interferometry, Classical Quantum Gravity **31**, 115010 (2014).
[33] S. Dimopoulos, P. W. Graham, J. M. Hogan, and M. A. Kasevich, Testing General Relativity with Atom Interferometry, Phys. Rev. Lett. **98**, 111102 (2007).
[34] J. Hartwig, S. Abend, C. Schubert, D. Schlippert, H. Ahlers, K. Posso-Trujillo, N. Gaaloul, W. Ertmer, and E. M. Rasel, Testing the universality of free fall with rubidium and ytterbium in a very large baseline atom interferometer, New J. Phys. **17**, 035011 (2015).
[35] P. Asenbaum, C. Overstreet, M. Kim, J. Curti, and M. A. Kasevich, Atom-Interferometric Test of the Equivalence Principle at the 10^{-12} Level, Phys. Rev. Lett. **125**, 191101 (2020).
[36] C. Schubert, D. Schlippert, S. Abend, E. Giese, A. Roura, W. P. Schleich, W. Ertmer, and E. M. Rasel, Scalable, symmetric atom interferometer for infrasound gravitational wave detection, arXiv:1909.01951.
[37] B. Canuel, A. Bertoldi, L. Amand, E. P. di Borgo, T. Chantrait, C. Danquigny, M. D. Álvarez, B. Fang, A. Freise, R. Geiger, J. Gillot, S. Henry, J. Hinderer, D. Holleville, J. Junca *et al.*, Exploring gravity with the MIGA large scale atom interferometer, Sci. Rep. **8**, 14064 (2018).
[38] B. Canuel, S. Abend, P. Amaro-Seoane, F. Badaracco, Q. Beaufils, A. Bertoldi, K. Bongs, P. Bouyer, C. Braxmaier, W. Chaibi, N. Christensen, F. Fitzek, G. Flouris, N. Gaaloul, S. Gaffet *et al.*, Elgar—A European laboratory for gravitation and atom-interferometric research, Classical Quantum Gravity **37**, 225017 (2020).
[39] B. Canuel, S. Abend, P. Amaro-Seoane, F. Badaracco, Q. Beaufils, A. Bertoldi, K. Bongs, P. Bouyer, C. Braxmaier, W. Chaibi, N. Christensen, F. Fitzek, G. Flouris, N. Gaaloul, S. Gaffet, C. L. G. Alzar *et al.*, Technologies for the Elgar large scale atom interferometer array, arXiv:2007.04014.
[40] S. Dimopoulos, P. W. Graham, J. M. Hogan, M. A. Kasevich, and S. Rajendran, Atomic gravitational wave interferometric sensor, Phys. Rev. D **78**, 122002 (2008).
[41] J. M. Hogan, D. M. S. Johnson, S. Dickerson, T. Kovachy, A. Sugarbaker, S.-w. Chiow, P. W. Graham, M. A. Kasevich, B. Saif, S. Rajendran, P. Bouyer, B. D. Seery, L. Feinberg, and R. Keski-Kuha, An atomic gravitational wave interferometric sensor in low Earth orbit (AGIS-LEO Collaboration), Gen. Relativ. Gravit. **43**, 1953 (2011).
[42] S. Loriani, D. Schlippert, C. Schubert, S. Abend, H. Ahlers, W. Ertmer, J. Rudolph, J. M. Hogan, M. A. Kasevich, E. M. Rasel, and N. Gaaloul, Atomic source selection in space-borne gravitational wave detection, New J. Phys. **21**, 063030 (2019).
[43] Y. A. El-Neaj, C. Alpigiani, S. Amairi-Pyka, H. Araújo, A. Balaž, A. Bassi, L. Bathe-Peters, B. Battelier, A. Belić, E. Bentine, J. Bernabeu, A. Bertoldi, R. Bingham, D. Blas, V. Bolpasi *et al.*, Aedge: Atomic experiment for dark matter and gravity exploration in space, Eur. Phys. J. Quantum Technol. **7**, 6 (2020).
[44] G. M. Tino, A. Bassi, G. Bianco, K. Bongs, P. Bouyer, L. Cacciapuoti, S. Capozziello, X. Chen, M. L. Chiofalo, A. Derevianko, W. Ertmer, N. Gaaloul, P. Gill, P. W. Graham, J. M. Hogan *et al.*, Sage: A proposal for a space atomic gravity explorer, Eur. Phys. J. D **73**, 228 (2019).
[45] B. Schrinski, K. Hornberger, and S. Nimmrichter, How to rule out collapse models with BEC interferometry, arXiv:2008.13580.
[46] F. Laloë and W. J. Mullin, Interferometry with independent Bose-Einstein condensates: Parity as an EPR/Bell quantum variable, Eur. Phys. J. B **70**, 377 (2009).
[47] T. Wasak and J. Chwedeńczuk, Bell Inequality, Einstein-Podolsky-Rosen Steering, and Quantum Metrology with Spinor Bose-Einstein Condensates, Phys. Rev. Lett. **120**, 140406 (2018).
[48] C. Gross, H. Strobel, E. Nicklas, T. Zibold, N. Bar-Gill, G. Kurizki, and M. K. Oberthaler, Atomic homodyne detection of continuous-variable entangled twin-atom states, Nature (London) **480**, 219 (2011).
[49] C. D. Hamley, C. S. Gerving, T. M. Hoang, E. M. Bookjans, and M. S. Chapman, Spin-nematic squeezed vacuum in a quantum gas, Nat. Phys. **8**, 305 (2012).

[50] Z. Zhang and L.-M. Duan, Generation of Massive Entanglement through an Adiabatic Quantum Phase Transition in a Spinor Condensate, Phys. Rev. Lett. **111**, 180401 (2013).

[51] X.-Y. Luo, Y.-Q. Zou, L.-N. Wu, Q. Liu, M.-F. Han, M. K. Tey, and L. You, Deterministic entanglement generation from driving through quantum phase transitions, Science **355**, 620 (2017).

[52] P. Feldmann, M. Gessner, M. Gabbrielli, C. Klempt, L. Santos, L. Pezzè, and A. Smerzi, Interferometric sensitivity and entanglement by scanning through quantum phase transitions in spinor Bose-Einstein condensates, Phys. Rev. A **97**, 032339 (2018).

[53] See Supplemental Material at http://link.aps.org/supplemental/10.1103/PhysRevLett.127.140402 for details on the quasiadiabatic state preparation, including Refs. [50–52,54–57].

[54] M.-S. Chang, C. D. Hamley, M. D. Barrett, J. A. Sauer, K. M. Fortier, W. Zhang, L. You, and M. S. Chapman, Observation of Spinor Dynamics in Optically Trapped ^{87}rb Bose-Einstein Condensates, Phys. Rev. Lett. **92**, 140403 (2004).

[55] S. R. Leslie, J. Guzman, M. Vengalattore, J. D. Sau, M. L. Cohen, and D. M. Stamper-Kurn, Amplification of fluctuations in a spinor Bose-Einstein condensate, Phys. Rev. A **79**, 043631 (2009).

[56] C. Klempt, O. Topic, G. Gebreyesus, M. Scherer, T. Henninger, P. Hyllus, W. Ertmer, L. Santos, and J. J. Arlt, Parametric Amplification of Vacuum Fluctuations in a Spinor Condensate, Phys. Rev. Lett. **104**, 195303 (2010).

[57] D. Linnemann, H. Strobel, W. Muessel, J. Schulz, R. J. Lewis-Swan, K. V. Kheruntsyan, and M. K. Oberthaler, Quantum-Enhanced Sensing Based on Time Reversal of Nonlinear Dynamics, Phys. Rev. Lett. **117**, 013001 (2016).

[58] Y. Castin and R. Dum, Bose-Einstein Condensates in Time Dependent Traps, Phys. Rev. Lett. **77**, 5315 (1996).

[59] H. Ammann and N. Christensen, Delta Kick Cooling: A New Method for Cooling Atoms, Phys. Rev. Lett. **78**, 2088 (1997).

[60] B. Lücke, J. Peise, G. Vitagliano, J. Arlt, L. Santos, G. Tóth, and C. Klempt, Detecting Multiparticle Entanglement of Dicke States, Phys. Rev. Lett. **112**, 155304 (2014).

[61] We are operating near the shot noise of the photo electrons and close to the full-well depth of the pixels. Therefore, technical improvements such as hardware binning are not beneficial to reduce the detection noise of extended atomic clouds in our system.

[62] B. K. Malia, J. Martínez-Rincón, Y. Wu, O. Hosten, and M. A. Kasevich, Free Space Ramsey Spectroscopy in Rubidium with Noise below the Quantum Projection Limit, Phys. Rev. Lett. **125**, 043202 (2020).

[63] P. Berg, S. Abend, G. Tackmann, C. Schubert, E. Giese, W. P. Schleich, F. A. Narducci, W. Ertmer, and E. M. Rasel, Composite-Light-Pulse Technique for High-Precision Atom Interferometry, Phys. Rev. Lett. **114**, 063002 (2015).

[64] D. L. Butts, K. Kotru, J. M. Kinast, A. M. Radojevic, B. P. Timmons, and R. E. Stoner, Efficient broadband Raman pulses for large-area atom interferometry, J. Opt. Soc. Am. B **30**, 922 (2013).

[65] K. Kotru, D. L. Butts, J. M. Kinast, and R. E. Stoner, Large-Area Atom Interferometry with Frequency-Swept Raman Adiabatic Passage, Phys. Rev. Lett. **115**, 103001 (2015).

[66] M. Jaffe, V. Xu, P. Haslinger, H. Müller, and P. Hamilton, Efficient Adiabatic Spin-Dependent Kicks in an Atom Interferometer, Phys. Rev. Lett. **121**, 040402 (2018).

[67] Other techniques, such as Bragg transitions or Bloch oscillations [68,69], can reach even better efficiencies but cannot be applied within our scheme.

[68] T. Kovachy, S.-w. Chiow, and M. A. Kasevich, Adiabatic-rapid-passage multiphoton Bragg atom optics, Phys. Rev. A **86**, 011606(R) (2012).

[69] S. Abend, M. Gebbe, M. Gersemann, H. Ahlers, H. Müntinga, E. Giese, N. Gaaloul, C. Schubert, C. Lämmerzahl, W. Ertmer, W. P. Schleich, and E. M. Rasel, Atom-Chip Fountain Gravimeter, Phys. Rev. Lett. **117**, 203003 (2016).

[70] In case we employ the information of the leftover atoms, these are added to the total atom number defining the shot noise of the ensemble. However, the total atom number changes by less than 1%, not causing a significant shift of the classical bound of our entanglement parameter.